Electrochemical and Spectroscopic Characterization of Manganese(III) Dodecaphenylporphyrin Derivatives and X-ray Structural Determination of Chloro(5,10,15,20-tetrakis(pentafluorophenyl)-2,3,7,8,12,13,17,18-octaphenylporphyrinato)-manganese(III). Formation of a Manganese(IV) Species by Ozone and Electrochemical Oxidation

Roger Guilard,*,† Karine Perié,† Jean-Michel Barbe,† Daniel J. Nurco,‡ Kevin M. Smith,*,‡ Eric Van Caemelbecke,§ and Karl M. Kadish*,§

LIMSAG (UMR 5633), Université de Bourgogne, Faculté des Sciences "Gabriel", 6 Boulevard Gabriel, 21000 Dijon, France, Department of Chemistry, University of California, Davis, California 95616, and Department of Chemistry, University of Houston, Houston, Texas 77204-5641

Received June 12, 1997

The electrochemistry of nine different manganese(III) dodecaphenylporphyrins containing halogen or CF_3 groups on the phenyl rings of the porphyrin macrocycle is reported. Six of the compounds were previously synthesized while three of the derivatives, (DPPF$_8$)MnCl, (DPPCl$_{12}$)MnCl and (DPPF$_{28}$)MnCl, are reported for the first time in this study. Each of the nine compounds was characterized in its neutral form by UV−visible and ^{1}H and ^{19}F NMR spectroscopy and in its singly oxidized form by UV−visible and ESR spectroscopy after reaction with ozone. An X-ray crystal structure of (DPPF$_{20}$)MnCl ($C_{92}H_{40}N_4F_{20}MnCl\cdot 2CHCl_3\cdot 0.25H_2O$) was also obtained. The compound crystallized in the monoclinic space group $P2_1/c$ with cell dimensions $a = 17.258(3)$ Å, $b = 28.593(6)$ Å, $c = 17.476(4)$ Å, $\beta = 107.16(2)°$, and $Z = 4$. It is nonplanar and adopts a saddle/ruffle hybridized macrocycle conformation.

Introduction

Ozone has been used for decades as an oxygen transfer agent in the oxidation of organic substrates.[1] This highly reactive oxidant has now replaced chlorine in the treatment of wastewater since chlorine and its chloro byproducts are extremely toxic for humans[2] and are strictly controlled in drinking water. Molecular ozone reacts with double bonds of molecules[3] as well as with other electron-rich sites[4] due to its electrophilic character.

Organic derivatives containing electron-withdrawing groups are not readily oxidized by ozone and advanced oxidation processes (AOP's) have therefore been developed[5] to facilitate the oxidative degradation of these types of compounds. The AOP's involve a combination of ozone and UV irradiation[6] or ozone and hydrogen peroxide.[5] During the AOP's, the ozone molecules decompose to give hydroxyl radicals. These extremely reactive species are nonselective and thus allow for a more efficient degradation of micropollutants. The treatment of wastewater by ozone now also involves new homogeneous/heteregeneous catalytic oxidation processes with metallic cations in solution[7] or on an alumina support.[8]

Meunier et al.[9,10] synthesized manganese and iron complexes of sulfonated tetraphenylporphyrins for use in the treatment of wastewater. These metalloporphyrins on a solid support were found to be very efficient catalysts in the degradation of poorly reactive organic compounds, such as polychlorophenols and related derivatives,[11] and have been used mainly with hydrogen peroxide or monopersulfate for the catalytic oxidation of difficult to degrade compounds in water. However, to our knowledge, there are no reports in the literature which describe ozonation reactions using metalloporphyrins as catalysts in the treatment of wastewater.

Metalloporphyrins such as (TPP)MnCl or (OEP)MnCl, where TPP and OEP are the dianions of tetraphenyl- and octaethylporphyrins, are rapidly bleached after oxidation by ozone at room temperature via an electrophilic attack on the electron-rich pyrrole double bonds. The group of Meunier[12] has investigated how ozone affects the chemical stability of tet-

† LIMSAG.
‡ University of California.
§ University of Houston.

(1) Bailey, P. S. In *Ozonation in Organic Chemistry*; Wasserman, H. H., Ed.; Academic Press: New York, 1982; Vol. 2, pp 3−422.
(2) Araujo, R. P. A.; Gasi, T. M. T.; Goldstein, E. G.; Amaral, L. A. V.; Francisco, R. *Proceedings of the Ozone in Wastewater Treatment & Industrial Applications*; Bollyky, L. J., Ed.; IOA: New York, 1989; Vol. 2, pp 221−230.
(3) Criegee, R. In *Peroxide Reaction Mechanisms*; Edwards, J. O., Ed.; Wiley-Interscience: New York, 1962.
(4) Bablon, G.; Bellamy, W. D.; Bourbigot, M. M.; Daniel, F. B.; Doré, M.; F., E.; Gordon, G.; Langlais, B.; Laplanche, A.; Ventresque, B. in *Ozone in Water Treatment*; Langlais, B.; Reckhow, A. Brink, D. R., Eds.; Lewis Publishers: Pearl River, NY, 1991; pp 11−132.
(5) Glaze, W. H.; Kang, J. W.; Chopin, D. H. *Ozone: Sci. Eng.* **1987**, *9*, 335−352.
(6) Peyton, G. R.; Glaze, W. H. *Environ. Sci. Technol.* **1988**, *22*, 761−767.
(7) Gracia, R.; Aragues, J. L.; Cortès, S.; Ovelleiro, J. L. *Proceedings of the 12th World Congress of the International Ozone Association*; IOA: Lille, 1995; Vol. 1, pp 75−86.
(8) Al−Hayek, N.; Legube, B.; Doré, M. *Environ. Technol. Lett.* **1989**, *10*, 415−426.
(9) Meunier, B.; Labat, G.; Seris, J. L. WO 91/08985, 1991.
(10) Meunier, B. *Chem. Rev. (Washington, D.C.)* **1992**, *92*, 1411−1456.
(11) Sorokin, A.; Seris, J.-L.; Meunier, B. *Science* **1995**, *268*, 1163−1166.
(12) Campestrini, S.; Robert, A.; Meunier, B. *J. Org. Chem.* **1991**, *56*, 6, 3725−3727.

S0020-1669(97)00717-9 CCC: $15.00
Published on Web 02/18/1998

ramesitylporphyrin (TMP) derivatives containing bromine substituents at the β-pyrrole positions. The brominated porphyrins are more stable than their unbrominated counterparts, and a high oxidation state reaction intermediate is observed during epoxidation of the olefins by ozone in the presence of (Br_8TMP)MnCl as a catalyst.

A number of dodecaphenylporphyrins have been synthesized and independently characterized by the laboratories of Smith[13−18] and Takeda.[19−21] The dodecaphenylporphyrins contain a phenyl ring at each β-pyrrole and *meso* position of the porphyrin macrocycle and are easier to synthesize than (Br_8TMP)MnCl which must be chromatographically separated from (Br_7TMP)MnCl and (Br_6TMP)MnCl, two products which are also formed in significant amounts during the synthesis.

Takeda and Sato[22] have optimized the synthesis of dodecaphenylporphyrins containing electron-withdrawing substituents on the phenyl rings located at the four *meso* positions of the porphyrin. The electron-withdrawing effect of the phenyl rings at the eight β-pyrrole positions of the porphyrin decreases the electron density on the pyrrole double bonds and thus limits the electrophilic attack of ozone. These derivatives are therefore, *a priori*, good candidates as catalysts for oxidation reactions involving ozone.

Recently, we reported the preliminary synthesis and characterization of manganese(III) dodecaphenylporphyrins having halogen- and CF_3-substituted phenyl groups at the four *meso* positions of the porphyrin.[23] In the present study, we examine the electrochemistry and ozonation reactions of these compounds and also report the synthesis, spectroscopic characterization, and ozonation of three new Mn(III) halogenated dodecaphenylporphyrin derivatives, ($DPPF_8$)MnCl (chloro(*meso*-tetrakis(2,6-difluorophenyl)octaphenylporphyrinato)manganese(III)), ($DPPCl_{12}$)MnCl (chloro(*meso*-tetrakis(2,3,5-trichlorophenyl)-octaphenylporphyrinato)manganese(III)), and ($DPPF_{28}$)MnCl (chloro(*meso*-tetrakis(pentafluorophenyl)-β-octakis(4-fluorophenyl)porphyrinato)manganese(III). An X-ray crystal structure of ($DPPF_{20}$)MnCl is also presented and shows that the compound is nonplanar and adopts a saddle/ruffle hybridized macrocycle conformation.

Experimental Section

Instrumentation. UV−visible spectra were performed with a Varian Cary I spectrophotometer. Infrared spectra of solid samples were obtained as a 1% dispersion in CsI using a Bruker IFS 66 V FTIR spectrophotometer. ^{1}H NMR spectra were recorded on a Bruker Avance DRX 500 spectrometer or on a Bruker AC200 of the "Centre de Spectrométrie Moléculaire" at the Université de Bourgogne in a 0.5 mL solution of $CDCl_3$, CD_2Cl_2, or DMSO-d_6 using nondeuterated solvent as an internal reference. ^{19}F NMR spectra were obtained on a Bruker AC200 spectrometer in a 0.5 mL solution of $CDCl_3$ using $CFCl_3$ as an internal reference. EPR spectra were performed on a Bruker ESP 300 spectrometer. The g values were measured relative to diphenylpicrylhydrazyl (dpph) ($g = 2.0037 \pm 0.002$). Mass spectra were obtained using a Kratos Concept 32 S of the "Centre de Spectrométrie Moléculaire" at the Université de Bourgogne in the LSIMS mode (liquid secondary ion mass spectrometry) using *m*-nitrobenzyl alcohol as matrix.

Cyclic voltammograms were obtained with an IBM model EC 225 voltammetric analyzer or an EG&G Princeton Applied Research model 273 potentiostat. Current−voltage curves were recorded on an EG&G Princeton Applied Research model RE-0151 X-Y recorder or a Zenith Data systems Model Z-386 SX/20 computer coupled with a Hewlett-Packard DeskJet 600 plotter. A three-electrode system was used, consisting of a glassy carbon or platinum button electrode, a platinum wire counter electrode, and a saturated calomel reference electrode (SCE). This reference electrode was separated from the bulk of the solution by a fritted-glass bridge filled with the solvent/supporting electrolyte mixture. All potentials are referenced to SCE.

X-ray Structural Determination of ($DPPF_{20}$)MnCl. Dark green parallelepipeds of ($DPPF_{20}$)MnCl were grown by the slow diffusion of *n*-hexane into a solution of the porphyrin dissolved in $CHCl_3$. The crystals were transferred directly from their mother liquor of crystallization to a light hydrocarbon oil (Paratone N) in which they were examined under a microscope, and a suitable specimen was selected. The selected crystal ($0.66 \times 0.40 \times 0.32$ mm) was mounted on a glass fiber and transferred to a 130(2) K stream of anhydrous nitrogen, supplied from a locally modified Nonius low-temperature apparatus, on a Siemens R3 m/V diffractometer equipped with graphite monochromated Mo Kα radiation from a normal-focus sealed tube operating at 2.0 kW. Data were collected to $2\theta_{max}$ of 45.0° in the index ranges $-2 \le h \le 19$, $-2 \le k \le 19$, and $-19 \le l \le 19$ with a total of 13 641 reflections collected including 10 773 independent reflections ($R_{int} = 0.038$). Calculations were performed on a Pentium 90 MHz processor with Siemens SHELXTL V. 5.03 software; scattering factors were used as provided with the software package. The structure was solved via direct methods and refined (based on $|F^2|$ using 10 764 independent reflections) with full-matrix least-squares methods. An empirical absorption correction was applied.[24] The core Mn and axial Cl were disordered in that as a pair they adopted two positions, with one Mn−Cl pair above the porphyrin mean plane, while an alternate Mn−Cl pair was found below the porphyrin mean plane. The two Mn−Cl pairs were refined with occupancies not varying among two atoms in a given pair and with the occupancies of the two pairs together summed to unity. This revealed one predominant Mn−Cl pair (Mn(1), Cl(1)) with 76.9(3)% occupancy and an alternate less occupied Mn−Cl pair (Mn(2), Cl(2)) present at 22.5(3)% occupancy. In close proximity to each of the axial Cl positions were partially occupied solvate species: O(23) (from solvate H_2O) was located 1.75(2) Å away from Cl(1) at 23.4(3)% occupancy, and Cl(4) (from solvate $CHCl_3$) was located 1.488(7) Å away from Cl(2) at 78.0(3)% occupancy. The occupancies of these solvate molecules, along with the occupancies of the axial chlorines to which they were in close proximity, were summed to unity. All non-hydrogen atoms were refined with anisotropic thermal parameters except for C(21) (from a $CHCl_3$) and O(23) (H_2O) which were refined with fixed isotropic thermal parameters. Phenyl rings were treated as rigid bodies. Hydrogen atom positions were generated by idealized geometry and refined using a riding model with isotropic thermal parameters of 1.2 times the thermal parameter of the attached carbon atom. (See Table 1 for experimental details).

Materials. Acetic acid, DMF, dichloromethane, toluene, pyridine, and benzonitrile were purchased from SDS, 1314 Peypin, France, or Acros Chemica and were used as received. For electrochemical measurements, benzonitrile (PhCN) was purchased from Aldrich Chemical Co. and distilled over P_2O_5 under vacuum prior to use. Absolute dichloromethane (CH_2Cl_2) and absolute pyridine (py) were purchased from Aldrich Chemical Co. and Fluka Chemika, respectively, and used without further purification. Tetra-*n*-butylammonium per-

(13) Medforth, C. J.; Smith, K. M. *Tetrahedron Lett.* **1990**, *31*, 5583−5586.
(14) Charlesworth, P.; Truscott, T. G.; Kessel, D.; Medforth, C. J.; Smith, K. M. *J. Chem. Soc., Faraday Trans* **1994**, *90*, 1073−1076.
(15) Medforth, C. J.; Hobbs, J. D.; Rodriguez, M. R.; Abraham, R. J.; Smith, K. M.; Shelnutt, J. A. *Inorg. Chem.* **1995**, *34*, 1333−1341.
(16) Shelnutt, J. A.; Medforth, C. J.; Berber, M. D.; Barkigia, K. M.; Smith, K. M. *J. Am. Chem. Soc.* **1991**, *113*, 4077−4087.
(17) Gentemann, S.; Medforth, C. J.; Forsyth, T. P.; Nurco, D. J.; Smith, K. M.; Fajer, J.; Holten, D. *J. Am. Chem. Soc.* **1994**, *116*, 7363−7368.
(18) Senge, M. O.; Forsyth, T. P.; Nguyen, L. T.; Smith, K. M. *Angew. Chem., Int. Ed. Engl.* **1994**, *33*, 2485−2487.
(19) Takeda, J.; Sato, M. *Tetrahedron Lett.* **1994**, *35*, 3565−3568.
(20) Takeda, J.; Sato, M. *Chem. Lett.* **1994**, 2233−2236.
(21) Takeda, J.; Ohya, T.; Sato, M. *Inorg. Chem.* **1992**, *31*, 2877−2880.
(22) Takeda, J.; Sato, M. *Chem. Pharm. Bull.* **1994**, *42*, 1005−1007.
(23) Perie, K.; Barbe, J. M.; Cocolios, P.; Guilard, R. *Bull. Soc. Chim. Fr.* **1996**, *133*, 697−702.
(24) Parkin, S. R.; Mazzi, B.; Hope, H. *J. Appl. Crystallogr.* **1995**, *28*, 53−56.

Table 1. Crystallographic Experimental Details

chem formula	$C_{92}H_{40}N_4F_{20}MnCl\cdot 2CHCl_3\cdot 0.25(H_2O)$
fw	1875.61
space group	$P2_1/c$ (No. 14)
a (Å)	17.258(3)
b (Å)	28.593(6)
c (Å)	17.476(4)
β (deg)	107.16(2)
V (Å^3)	8420(3)
Z	4
T (K)	130(2)
λ (Å)	0.710 73
ρ_{calc} (g cm^{-3})	1.512
μ (mm^{-1})	0.453
min transm	0.77
max transm	0.89
R1(F_o^2)($>2\sigma(I)$)[a]	0.066
wR2(F_o^2)(all data)[a]	0.193

[a] $R1 = \sum||F_o| - |F_c||/\sum|F_o|$ and $wR2 = [\sum[w(F_o^2 - F_c^2)^2]/\sum[w(F_o^2)^2]]^{1/2}$; $w = 1/[\sigma^2(F_o^2) + (0.0865P)^2 + 24.3094P]$, where $P = (F_o^2 + 2F_c^2)/3$.

chlorate was purchased from Sigma Chemical Co., recrystallized from ethyl alcohol, and dried under vacuum at 40 °C for at least 1 week prior to use. The $(DPPF_4)H_2$, $(DPP(CF_3)_4)H_2$, $(DPPBr_4)H_2$, $(DPPCl_8)H_2$, and $(DPPF_{20})H_2$ derivatives, as well as their Mn(III) analogues, were synthesized using previously described procedures.[23] ^{19}F NMR data for these compounds are as follows: $(DPPF_4)H_2$, δ (ppm) −116.95 (*meso*-PhF_p, $^3J_{FH}$ = 9.5 Hz; $^4J_{FH}$ = 5.9 Hz); $(DPPF_4)$MnCl, δ (ppm) −117.52 (*meso*-PhF_p); $(DPP(CF_3)_4)H_2$, δ (ppm) −63.54 (CF_3); $(DPP(CF_3)_4)$MnCl, δ (ppm) −64.15 (CF_3); $(DPPF_{20})H_2$, δ (ppm) −136.17 (*meso*-PhF_o, J_{FmFo} = 27.6 Hz), −154.78 (*meso*-PhF_p, J_{FmFp} = 21.6 Hz), −165.47 (*meso*-PhF_m, J_{FmFo} = 27.6 Hz; J_{FmFp} = 21.6 Hz); $(DPPF_{20})$MnCl, δ (ppm) −124.17 (*meso*-PhF_o), −154.12 (*meso*-PhF_p), −160.23 (*meso*-PhF_m).

***meso*-Tetrakis(2,6-difluorophenyl)octaphenylporphyrin, $(DPPF_8)H_2$.** A solution containing 3,4-diphenylpyrrole (1.8 g, 8.2 mmol) and 2,6-difluorobenzaldehyde (886 mL, 8.2 mmol) in 1 L of dichloromethane was purged with N_2 for 10 min after which boron trifluoride etherate (0.5 mL, 4 mmol) was added. The condensation reaction was performed at room temperature for 24 h. After evaporation of the solvent, the mixture was refluxed for 2 h with 2,3-dichloro-5,6-dicyano-1,4-benzoquinone (1.5 g, 6.7 mmol) in 500 mL of toluene. Triethylamine (1 mL, 7.2 mmol) was then added at room temperature to recover the free-base porphyrin. After evaporation of the solvent, the crude product was purified by two successive columns on silica. Elution with a dichloromethane/heptane mixture (50/50 by volume) gave the desired porphyrin. A partial evaporation of the solvent followed by addition of pentane led to precipitation of the porphyrin. After filtration, 2.3 g (81% yield) of $(DPPF_8)H_2$ was obtained. Anal. Calcd for $C_{92}H_{54}N_4F_8$: C, 80.8; H, 4.0; N, 4.1; F, 11.1. Found: C, 79.3; H, 4.0; N, 3.9; F, 10.5. MS (LSIMS): m/z 1368, $[M + H]^+$, 100. ^{1}H NMR ($CDCl_3$, 200 MHz): δ (ppm) −1.09 (2H, s, NH), 6.18 (8H, dd, *meso*-PhH_m, J_{HmHp} = 8.5 Hz, $^3J_{HF}$ = 7 Hz), 6.68 (4H, t, *meso-PhH*$_p$, J_{HpHm} = 8.5 Hz), 6.73−6.78 (24H, m, β-Ph$H_{m,p}$), 6.90 (16H, m, β-PhH_o). ^{19}F NMR ($CDCl_3$): δ (ppm) −108.55 (*meso*-PhF_o, $^3J_{FH}$ = 7 Hz). UV−visible (CH_2Cl_2) [λ_{max}, nm ($10^{-3}\epsilon$, mol^{-1} L cm^{-1})]: 452 (215), 546 (17.6), 624 (7.3), 689 (2.4). IR (CsI): ν (cm^{-1}) 3327 for ν_{NH}.

Chloro(*meso*-tetrakis(2,6-difluorophenyl)octaphenylporphyrinato)-manganese(III), $(DPPF_8)$MnCl. $(DPPF_8)H_2$ (300 mg, 0.21 mmol) was dissolved in 70 mL of benzonitrile after which manganese(II) chloride tetrahydrate (210 mg, 1 mmol) was added and the mixture was refluxed for 2 h. After evaporation of the solvent, the product was dissolved in 500 mL of dichloromethane and washed with water. The solution was dried on magnesium sulfate and evaporated to dryness. The crude product was purified by column chromatography on a silica gel column and eluted with dichloromethane. Partial evaporation of the solvent and addition of pentane led to precipitation of the porphyrin. After filtration, 172 mg (54% yield) of $(DPPF_8)$MnCl was obtained. Anal. Calcd for $C_{92}H_{52}N_4F_8MnCl$: C, 75.9; H, 3.6; N, 3.8. Found: C, 73.2; H, 3.6; N, 3.8. MS (LSIMS): m/z 1419, $[M - Cl]^+$, 100. ^{1}H NMR ($CDCl_3$, 500 MHz): δ (ppm) 6.57, 7.10, 8.07, 8.45. ^{19}F NMR ($CDCl_3$): δ (ppm) −102.5 (*meso*-PhF_o). UV−visible (CH_2Cl_2) [λ_{max}, nm ($10^{-3}\epsilon$, mol^{-1} L cm^{-1})]: 382 (59), 490 (71.5), 593 (11.2), 639 (8.9); IR (CsI): ν (cm^{-1}): 294 for ν_{MnCl}.

***meso*-Tetrakis(2,3,5-trichlorophenyl)octaphenylporphyrin, $(DPPCl_{12})H_2$.** The synthesis was performed using the method described above for $(DPPF_8)H_2$ starting from 3,4-diphenylpyrrole (1 g, 4.8 mmol), 2,3,5-trichlorobenzaldehyde (1 g, 4.8 mmol), and boron trifluoride etherate (0.45 mL, 3.6 mmol) in 750 mL of dichloromethane. A 740 mg amount of $(DPPCl_{12})H_2$ (38% yield) was obtained. Anal. Calcd for $C_{92}H_{50}N_4Cl_{12}$: C, 67.5; H, 3.1; N, 3.4; Cl, 26.0. Found: C, 66.2; H, 3.2; N, 3.2; Cl, 24.6. MS (LSIMS): m/z 1635, $[M + H]^+$, 100. ^{1}H NMR ($CDCl_3$, 200 MHz): δ (ppm) −1.32 (2H, s, NH), 6.06 (4H, m, *meso*-PhH_p), 6.85−6.93 (24H, m, β-Ph$H_{m,p}$), 7.08 (16H, m, β-PhH_o), 7.27 (4H, m, *meso*-PhH_o). UV−visible (CH_2Cl_2) [λ_{max}, nm ($10^{-3}\epsilon$, mol^{-1} L cm^{-1})] 459 (165), 552 (14.8), 629 (6.3), 695 (2.3). IR (CsI): ν (cm^{-1}) 3330 for ν_{NH}.

Chloro(*meso*-tetrakis(2,3,5-trichlorophenyl)octaphenylporphyrinato)manganese(III), $(DPPCl_{12})$MnCl. The synthesis was performed using the method described above for $(DPPF_8)$MnCl starting from $(DPPCl_{12})H_2$ (450 mg, 0.27 mmol) and manganese(II) chloride tetrahydrate (270 mg, 1.37 mmol) in 100 mL of benzonitrile to give 280 mg (60%) of $(DPPCl_{12})$MnCl. Anal. Calcd for $C_{92}H_{48}N_4MnCl_{13}$: C, 64.1; H, 2.8; N, 3.2. Found: C, 64.1; H, 3.0; N, 3.3. MS (LSIMS): m/z 1689, $[M - Cl]^+$, 100. ^{1}H NMR ($CDCl_3$, 500 MHz): δ (ppm) 6.68, 7.46, 8.88. UV−visible (CH_2Cl_2): [λ_{max}, nm ($10^{-3}\epsilon$, mol^{-1} L cm^{-1})]: 384 (59.1), 501 (81.4), 602 (12.3), 644 (7.5). IR (CsI): ν (cm^{-1}) 282 for ν_{MnCl}.

***meso*-Tetrakis(pentafluorophenyl)-β-octakis(4-fluorophenyl)porphyrin, $(DPPF_{28})H_2$.** The synthesis was performed using the method described above for $(DPPF_8)H_2$ starting from 3,4-bis(4-fluorophenyl)-pyrrole[25] (500 mg, 2 mmol), pentafluorobenzaldehyde (0.24 mL, 2 mmol), and boron trifluoride etherate (0.2 mL, 1.6 mmol) in 250 mL of dichloromethane to give 150 mg (17% yield) of $(DPPF_{28})H_2$. ^{1}H NMR ($CDCl_3$, 500 MHz): δ (ppm) −1.51 (2H, s, NH), 6.73 (16H, t, β-PhH_m, J_{HmHo} = 3.4 Hz, $^3J_{HF}$ = 3.4 Hz), 6.93 (8H, d, β-PhH_o), 6.96 (8H, d β-Ph$H_{o'}$). ^{19}F NMR ($CDCl_3$): δ (ppm) −136.14 (*meso*-PhF_o, J_{FmFo} = 26.4 Hz), −153.02 (*meso*-PhF_p, J_{FmFp} = 21.6 Hz), −164.42 (*meso*-PhF_m, J_{FmFo} = 26.4 Hz; J_{FmFp} = 21.6 Hz), −113.68 (β−PhF_p). UV−visible (CH_2Cl_2) [λ_{max}, nm ($10^{-3}\epsilon$, mol^{-1} L cm^{-1})]: 443 (178), 538 (17.6), 617 (7.4). IR (CsI): ν (cm^{-1}) 3327 for ν_{NH}.

Chloro(*meso*-tetrakis(pentafluorophenyl)-β-octakis(4-fluorophenyl)- porphyrinato)manganese(III), $(DPPF_{28})$MnCl. The synthesis was performed using the method described above for $(DPPF_8)$MnCl starting from $(DPPF_{28})H_2$ (100 mg, 0.058 mmol) and manganese(II) chloride tetrahydrate (60 mg, 0.3 mmol) in 30 mL of benzonitrile to give 68 mg (65%) of $(DPPF_{28})$MnCl. ^{1}H NMR (CD_2Cl_2, 500 MHz): δ (ppm) 7.22, 7.27, 8.34. ^{19}F NMR ($CDCl_3$): δ (ppm) −101.32 (*meso*-PhF_o), −96.59 (*meso*-PhF_o), −150.62 (*meso*-PhF_p), −154.57 (*meso*-PhF_m). UV−visible (CH_2Cl_2) (λ_{max}, nm): 379, 479, 590, 534. IR (CsI): ν (cm^{-1}) 306 for ν_{MnCl}.

Results and Discussion

Synthesis. The structures of porphyrin macrocycles for the investigated compounds are given in Chart 1.

The syntheses of 2,3,5,7,8,10,12,13,15,17,18,20-dodecaphenylporphyrin, (DPP)MnCl, and the more sterically hindered substituted derivatives, $(DPPF_4)$MnCl, $(DPP(CF_3)_4)$MnCl, $(DPPBr_4)$MnCl, $(DPPCl_8)$MnCl, and $(DPPF_{20})$MnCl, have previously been reported.[23] The free-base porphyrins, $(DPPF_8)H_2$ and $(DPPCl_{12})H_2$, were synthesized according to the method described by Takeda et al.[22]

A condensation of 3,4-diphenylpyrrole with equivalent amounts of the corresponding aldehyde in dichloromethane was followed by oxidation with 2,3-dichloro-5,6-dicyano-1,4-benzoquinone in refluxing toluene to give the free-base porphyrin.[13]

(25) Nurco, D. J.; Smith, K. M. Unpublished results.

Chart 1

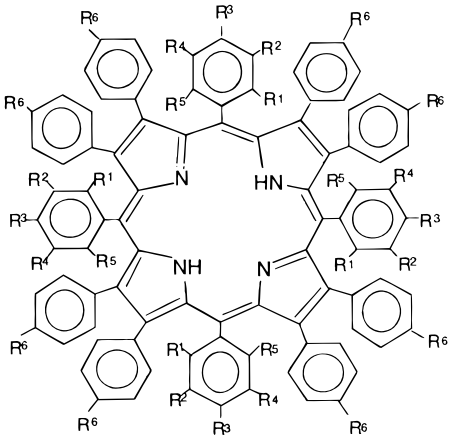

$R^1 = R^2 = R^3 = R^4 = R^5 = R^6 = H$	$P = (DPP)H_2$
$R^1 = R^2 = R^4 = R^5 = R^6 = H, R^3 = F$	$P = (DPPF_4)H_2$
$R^1 = R^2 = R^4 = R^5 = R^6 = H, R^3 = Br$	$P = (DPPBr_4)H_2$
$R^1 = R^2 = R^4 = R^5 = R^6 = H, R^3 = CF_3$	$P = (DPP(CF_3)_4)H_2$
$R^1 = R^5 = F, R^2 = R^3 = R^4 = R^6 = H$	$P = (DPPF_8)H_2$
$R^1 = R^5 = Cl, R^2 = R^3 = R^4 = R^6 = H,$	$P = (DPPCl_8)H_2$
$R^1 = R^2 = R^4 = Cl, R^3 = R^5 = R^6 = H$	$P = (DPPCl_{12})H_2$
$R^1 = R^2 = R^3 = R^4 = R^5 = F, R^6 = H$	$P= (DPPF_{20})H_2$
$R^1 = R^2 = R^3 = R^4 = R^5 = R^6 = F$	$P = (DPPF_{28})H_2$

The synthesis of $(DPPF_{28})H_2$ was performed by condensation of equimolar 3,4-bis(4-fluorophenyl)pyrrole and pentafluorobenzaldehyde while 3,4-bis(4-fluorophenyl)pyrrole was produced via condensation of *N*-(dimethylacetyl)iminodiacetate with 4,4′-difluorobenzil in alkaline media.[25] The free-base porphyrins were all metalated with manganese(II) chloride tetrahydrate in refluxing benzonitrile. The desired chloromanganese(III) complexes were obtained after purification on a silica column and further hydrogen chloride bubbling in the solution of the complex. The yields are given in the Experimental Section.

UV−Visible Spectra. UV−visible data of the investigated Mn(III) porphyrins and the starting free-base derivatives are given in the Experimental Section. Each free-base porphyrin is characterized by a single Soret band between 443 and 468 nm and three Q-bands between 538 and 729 nm. The exact position of these absorption bands depends upon the degree of substitution on the phenyl rings bound to the porphyrin skeleton. For example, the Soret band of $(DPPF_8)H_2$ is located at 452 nm and is blue shifted by 10 nm with respect to the Soret band of $(DPPCl_8)H_2$ (λ = 462 nm)[23] under the same solution conditions. This result indicates that the substitution by eight fluorine atoms in the ortho position of the *meso*-phenyl groups leads to an increase of the HOMO−LUMO gap as compared to the HOMO−LUMO gap for the DPP macrocycle with eight chlorine atoms.

The investigated dodecaphenylporphyrins have sterically hindered phenyl groups in the *meso* and β-pyrrole positions of the macrocycle and thus have a nonplanar conformation similar to that of β-pyrrole perhalogenated porphyrins. It is known that steric hindrance in the porphyrin structure will modify the orbital diagram by decreasing the HOMO−LUMO gap[26] and the same stabilization of the LUMO and HOMO orbitals can be induced by increasing the electronegativity of the groups at the β-pyrrole positions of the porphyrins. The difference in Soret band position of $(DPPF_8)H_2$ and $(DPPCl_8)H_2$ (452 and 462 nm) might be explained by a smaller deformation of the $(DPPF_8)H_2$ macrocycle due to the smaller steric effect of the fluorine atoms (resulting in a red shift of the $(DPPCl_8)H_2$ bands) or by a greater stabilization of the HOMO orbitals as compared to the LUMO orbitals in $(DPPF_8)H_2$.[22] However, only small differences in λ_{max} are seen between the Soret bands of $(DPPCl_8)H_2$ (462 nm) and $(DPPCl_{12})H_2$ (459 nm) and virtually no spectral changes are observed between $(DPPF_{20})H_2$ (444 nm) and $(DPPF_{28})H_2$ (443 nm) which have nearly identical spectra despite the fact that the latter compound has been substituted at the β-phenyl groups. A similar lack of substituent effect has previously been reported for porphyrins with different *para*-substituted *meso*-phenyl groups.[23]

The λ_{max} values of each chloromanganese(III) complex are given in the Experimental Section or in the literature.[23] All of the compounds exhibit a hyperporphyrin pattern, and the absorption bands are red shifted with respect to planar porphyrins such as those with OEP or TPP macrocycles.

^{1}H and ^{19}F NMR Spectra. The ^{1}H NMR data are given in the Experimental Section. The protons at the meta position in the *meso*-phenyl groups of $(DPPF_8)H_2$ are more shielded than the same protons in $(DPPCl_8)H_2$. A similar difference in shielding is seen for the ortho protons of substituted benzene derivatives when fluorine or chlorine atoms are added to the ring. On the other hand, the *meso*-phenyl protons in the para position of $(DPPF_8)H_2$ are deshielded compared to the same protons in $(DPPCl_8)H_2$. This behavior is consistent with the observed results for the ortho protons. The F atoms located at the ortho position in the *meso*-phenyl groups, as well as those at the para positions of the β-phenyl groups produce a similar effect on the NMR resonance signals of the remaining phenyl protons.

Resonances of the iminic protons show a larger decrease of the ring current upon substitution of the β-pyrrole positions by phenyl groups as compared to substitution at these positions by bromine atoms. The resonances of the iminic protons occur at −1.09 ppm for $(DPPF_8)H_2$ and −1.32 ppm for $(DPPCl_{12})H_2$, and this suggests a smaller macrocycle deformation in $(DPPCl_{12})H_2$ than $(DPPF_8)H_2$ which balances the increase of electron-withdrawing substituents.

The free-base DPP derivatives with fluorine atoms at the para position of the *meso*-phenyl rings are characterized by a single resonance signal in ^{19}F NMR while two signals are seen for the derivatives with fluorine atoms at the meta and ortho positions of the phenyl rings (see Experimental Section). The spectrum of $(DPP(CF_3)_4)H_2$ exhibits a singlet at −63.5 ppm which corresponds to 12 fluorine atoms. The spectrum of $(DPPF_4)H_2$ exhibits a triplet of triplets at −116.9 ppm which results from a coupling with hydrogen atoms in the meta ($^3J_{HF}$ = 9.5 Hz) and ortho positions ($^4J_{HF}$ = 5.9 Hz). Triplets for fluorine atoms at the para position of the *meso*-phenyl groups are observed at ∼−154.8 for $(DPPF_{20})H_2$ and −153.0 ppm for $(DPPF_{28})H_2$ and result from a coupling with the fluorine atoms in the meta position ($^3J_{FF}$ = 21.6 Hz). The fluorine atoms at the ortho and ortho′ position in the *meso*-phenyl groups appear as two doublets at ∼−108 ppm ($^3J_{FH}$ = 7 Hz) for $(DPPF_8)H_2$ and −136 ppm ($^3J_{FF}$ = 27.6, 26.4 Hz) for $(DPPF_{20})H_2$ and $(DPPF_{28})H_2$. No coupling is detected between the fluorine atoms at the para position of the β-pyrrole phenyl rings and protons on the same ring.

(26) Takeuchi, T.; Gray, H. B.; Goddard, W. A., III. *J. Am. Chem. Soc.* **1994**, *116*, 9730−9732.

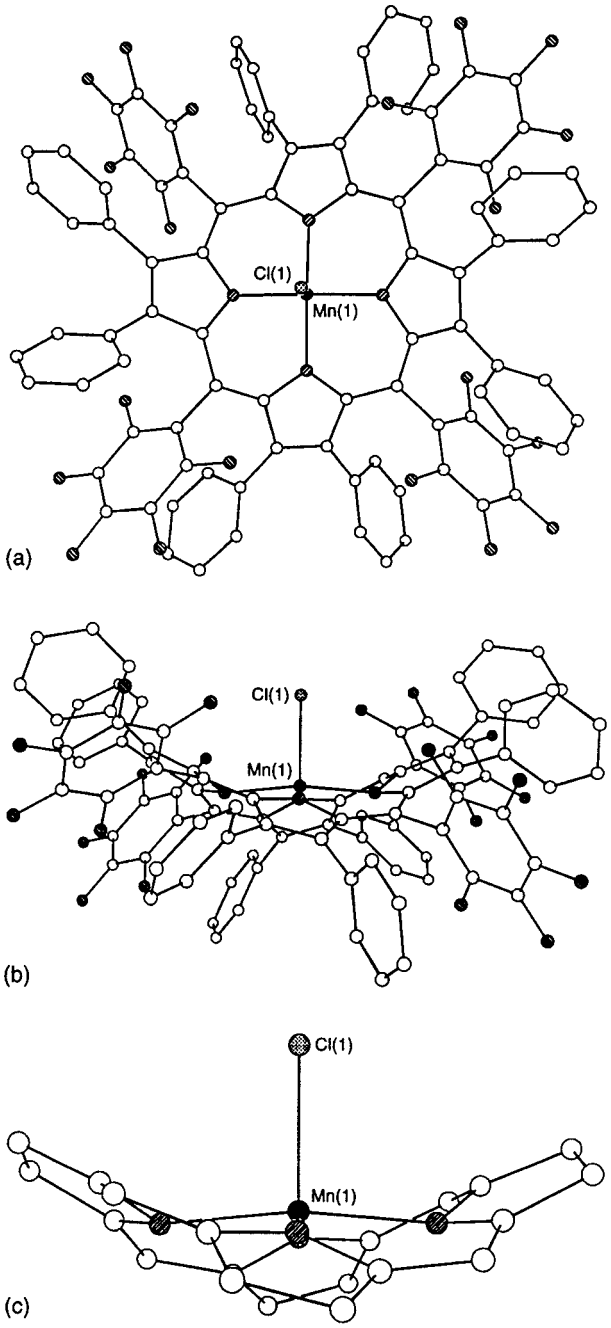

Figure 1. Molecular structure of $(DPPF_{20})MnCl$: (a) top view; (b) side view; (c) side view with phenyl substituents removed.

The ^1H NMR spectra of the manganese(III) derivatives are difficult to interpret since the paramagnetism of the metal ion induces a large broadening of the resonance signals. The chloromanganese(III) porphyrins also exhibit broad ^{19}F NMR signals for the fluorine atoms at the ortho position of the *meso*-phenyl groups which are close to the metal center. In contrast, the chemical shifts of the fluorine atoms of the *meso*-phenyl rings are unaffected by the presence of the paramagnetic Mn(III) center and a resonance is not observed for fluorine atoms at the para position of the β-pyrrole phenyl groups (see Experimental Section).

X-ray Crystallography. The crystal structure of $(DPPF_{20})MnCl$ (Figure 1) reveals a nonplanar conformation of the macrocycle as expected for this type of peripherally congested porphyrin. The macrocycle exhibits a C_β maximum deviation of 1.176(5) Å and an average macrocycle atom deviation of 0.528 Å from the porphyrin mean plane (herein "porphyrin mean plane" refers to the least-squares plane calculated for the 24 carbon and nitrogen atoms of the porphyrin macrocycle). These deviations and the numbering scheme used are shown in Figure 2. The macrocycle displays a mixture of saddle/ruffle hybridized distortions[27] as evidenced by the out of plane displacements (Figure 1), Cα−N−N−Cα torsion angles[28] (Table 2), and pyrrole tilt angles (Table 3). Nonplanar conformations of this type have been observed in previous porphyrin crystal structures, notably in one of two reported crystalline forms of $(DPPF_{20})Ni^{II}$ [29] which is very similar to this structure, and to a slightly lesser extent in (2,3,7,8,12,13,17,18-octabromo-5,10,15,20-tetramesitylporphyrinato)nickel(II)[30] and chloro(2,3,7,8,12,13,17,18-octabromo-5,10,15,20-tetramesitylporphyrinato)iron(III).[31] An average Mn−N bond length of 1.99(1) Å and a Mn−Cl bond length of 2.369(3) Å were observed; these values are similar to the analogous bond lengths observed in previously reported $Mn^{III}Cl$ porphyrin crystal structures.[32,33]

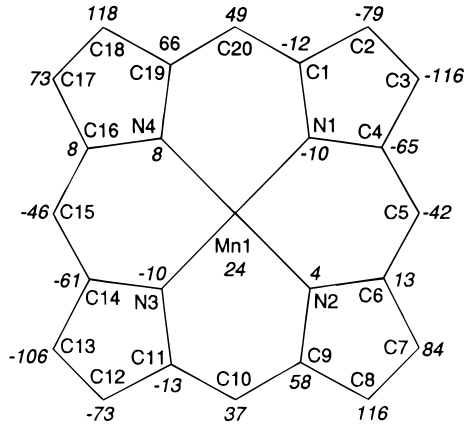

Figure 2. Numbering scheme and displacements of the macrocycle atoms (in Å × 100) from the porphyrin mean plane (calculated for the 24 core carbon and nitrogen atoms) for $(DPPF_{20})MnCl$.

Table 2. Cα−N−N−Cα Torsion Angles

Cα−N−N−Cα	torsion angle (deg)	Cα−N−N−Cα	torsion angle (deg)
C(1)−N(1)−N(3)−C(14)	24.3(5)	C(6)−N(2)−N(4)−C(19)	24.9(5)
C(4)−N(1)−N(3)−C(11)	27.2(5)	C(9)−N(2)−N(4)−C(16)	27.7(5)

Ozone Oxidation. Each DPP complex was dissolved in CH_2Cl_2 (0.02 mmol in 5 mL of solvent) and exposed to ozone ($[O_3] = 40$ g/m^3, flow rate = 15 mL/min). The UV−visible spectra were recorded both before and after the ozonation reaction, and an example of the resulting spectral changes is shown in Figure 3a for the case of $(DPPF_{20})MnCl$. Similar UV−vis spectra were observed upon reaction of ozone with each dodecaphenylpor-

(27) Scheidt, W. R.; Lee, Y. J. *Struct. Bonding* **1987**, *64*, 1−70.
(28) Hobbs, J. D.; Majumder, S. A.; Luo, L.; Sickelsmith, G. A.; Quirke, J. M. E.; Medforth, C. J.; Smith, K. M.; Shelnutt, J. A. *J. Am. Chem. Soc.* **1994**, *116*, 3261−3270.
(29) Nurco, D. J.; Medforth, C. J.; Forsyth, T. P.; Olmstead, M. M.; Smith, K. M. *J. Am. Chem. Soc.* **1996**, *118*, 10918−10919.
(30) Mandon, D.; Ochsenbein, P.; Fisher, J.; Weiss, R.; Jayaraj, K.; Austin, R. N.; Gold, A.; White, P. S.; Brigaud, O.; Battioni, P.; Mansuy, D. *Inorg. Chem.* **1992**, *31*, 2044−2049.
(31) Ochsenbein, P.; Mandon, D.; Fisher, J.; Weiss, R.; Austin, R.; Jayaraj, J.; Gold, A.; Terner, J.; Bill, E.; Müther, M.; Trautwein, A. X. *Angew. Chem., Int. Ed. Engl.* **1993**, *32*, 1437−1439.
(32) Guilard, R.; Brandès, S.; Tabard, A.; Bayeul, D.; Lecomte, C.; Richard, P.; Latour, J.-M. *J. Am. Chem. Soc.* **1994**, *116*, 10202−10211.
(33) Tulinsky, A.; Chen, B. M. L. *J. Am. Chem. Soc.* **1977**, *99*, 3647−3651.

Table 3. Selected Dihedral Angles for (DPP F_{20})MnCl

plane 1	plane 2	plane 1−plane 2 dihedral angle (deg)
N(1),C(1),C(2),C(3),C(4)	porphyrin mean plane	28.5(2)
N(2),C(6),C(7),C(8),C(9)	porphyrin mean plane	29.3(2)
N(3),C(11),C(12),C(13),C(14)	porphyrin mean plane	25.3(1)
N(4),C(16),C(17),C(18),C(19)	porphyrin mean plane	29.3(1)
N(1),C(1),C(2),C(3),C(4)	N(3),C(11),C(12),C(13),C(14)	53.8(2)
N(2),C(6),C(7),C(8),C(9)	N(4),C(16),C(17),C(18),C(19)	58.4(2)
N(1),C(1),C(2),C(3),C(4)	N(2),C(6),C(7),C(8),C(9)	42.3(2)
N(2),C(6),C(7),C(8),C(9)	N(3),C(11),C(12),C(13),C(14)	35.2(2)
N(3),C(11),C(12),C(13),C(14)	N(4),C(16),C(17),C(18),C(19)	37.1(2)
N(4),C(16),C(17),C(18),C(19)	N(1),C(1),C(2),C(3),C(4)	41.4(2)

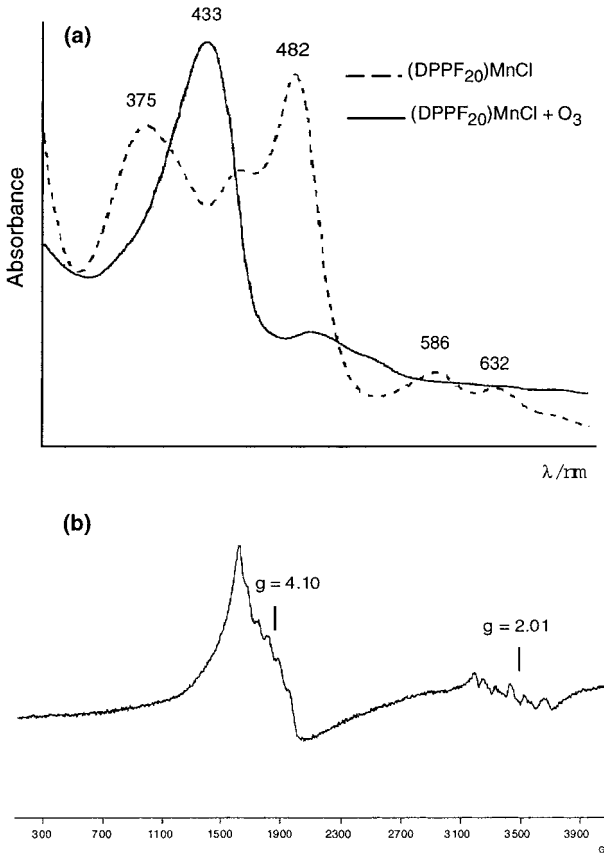

Figure 3. (a) Room-temperature UV−visible spectra of (DPPF$_{20}$)MnCl before (- - -) and after (—) reaction with O_3 in CH_2Cl_2 and (b) ESR spectrum of the ozonation product in CH_2Cl_2 at 80 K.

Table 4. UV−Visible (λ_{max}, Soret Band) and ESR Data for Ozonated Complexes

species	λ_{max}, nm	*g*	
(DPPF$_4$)MnCl + O_3	443	*a*	
(DPPBr$_4$)MnCl + O_3	442	3.94	2.00
(DPP(CF$_3$)$_4$)MnCl + O_3	440	3.99	2.00
(DPPF$_8$)MnCl + O_3	436	4.02	2.00
(DPPCl$_8$)MnCl + O_3	449	4.04	2.01
(DPPCl$_{12}$)MnCl + O_3	439	4.03	2.00
(DPPF$_{20}$)MnCl + O_3	433	4.10	2.01
(DPPF$_{28}$)MnCl + O_3	438	*a*	

[a] ESR spectrum not recorded.

phyrin, the only exception being (DPP)MnCl which is immediatly bleached during the reaction (see Table 4). This result seems to show that a substitution on the *meso*-phenyl groups by electron-withdrawing moieties will stabilize the macrocycle toward ozone. No degradation of the compounds was observed during the time of ozonation (ca 30 min), but a kinetic study of this reaction was not carried out.

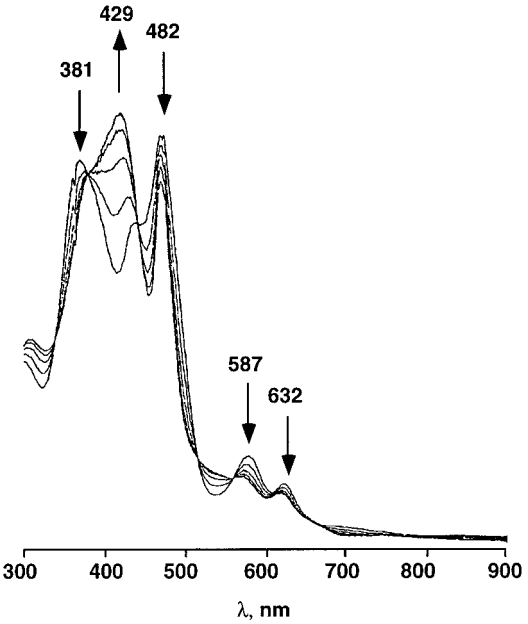

Figure 4. Time-resolved thin-layer electronic absorption spectra obtained by kinetics after the first oxidation of (DPPF$_{20}$)MnCl in CH_2Cl_2, 0.2 M TBAP.

The UV−visible spectra of the ozonated derivatives resemble those of manganese(IV) porphyrins,[34−38] and this is also the case for the ESR spectra of the ozonated complexes all of which have signals around $g = 2$ and 4 (see Table 4 and Figure 3b) and are characteristic of manganese(IV) porphyrins.[39] The high oxidation state compounds are stable under ozone but return to a manganese(III) form of the complex when ozone is no longer passed through the solution.

Electrooxidation. Attempts were made to electrochemically generate and spectrally characterize the high oxidation state manganese dodecaphenylporphyrins for comparison with results from the ozonation reactions, and an example of the resulting thin-layer spectra obtained during the conversion of (DPPF$_{20}$)MnCl to its singly oxidized product is shown in Figure 4. The spectrum of the oxidized product in CH_2Cl_2 containing 0.1 M TBAP is characterized by a Soret band at 429 nm as compared to a Soret band maximum of 433 nm for the same manganese

(34) Bortolini, O.; Meunier, B. *J. Chem. Soc., Chem. Commun.* **1983**, 1364−1366.
(35) Bortolini, O.; Ricci, M.; Meunier, B.; Friant, P.; Ascone, I.; Goulon, J. *New J. Chem.* **1986**, *10*, 39−49.
(36) Willner, I.; Otvos, J. W.; Calvin, M. *J. Chem. Soc., Chem. Commun.* **1980**, 964−965.
(37) Camenzind, M. J.; Hollander, F. J.; Hill, C. L. *Inorg. Chem.* **1982**, *21*, 1, 4301−4308.
(38) Groves, J. T.; Stern, M. K. *J. Am. Chem. Soc.* **1987**, *109*, 3812−3814.
(39) Camenzind, M. J.; Hollander, F. J.; Hill, C. L. *Inorg. Chem.* **1983**, *22*, 2, 3776−3784.

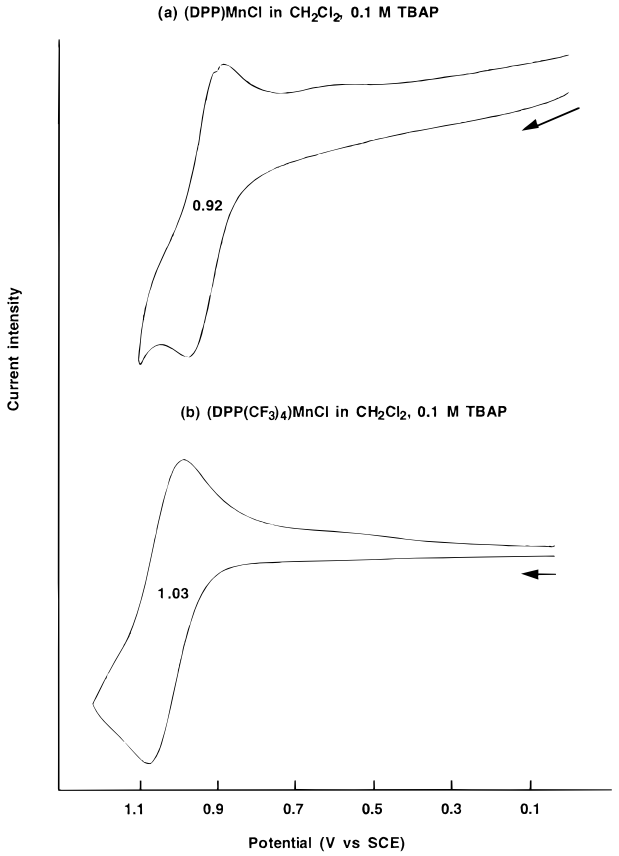

Figure 5. Cyclic voltammograms showing the first oxidation of (a) (DPP)MnCl and (b) (DPP(CF_3)$_4$)MnCl in CH_2Cl_2, 0.1 M TBAP.

porphyrin after reaction with ozone (see Figure 3a). The similarity of the two spectra suggests that a Mn(IV) species can also be generated via a simple electochemical reaction.

Unfortunately, a lack of stability of the singly oxidized species is observed at time scales longer than a few seconds and this is also the case for the other compounds, all of which undergo a rapid chemical reaction after electrooxidation in PhCN or CH_2Cl_2 containing 0.1 M TBAP. The rate of the chemical reaction varies with the degree of macrocyle substitution and the nature of the solvent, and in some cases not even a single well-defined oxidation can be observed on the cyclic voltammetry time scale. The exact nature of the chemical product(s) which is (are) present in solution after the initial oxidation is not known, and this point was not further investigated after obtaining half-wave or peak potentials for the initial electron-transfer reaction.

The first oxidation in PhCN is reversible to quasireversible for (DPP)MnCl, (DPPF$_4$)MnCl, (DPPBr$_4$)MnCl, (DPP(CF_3)$_4$)MnCl, and (DPPCl$_8$)MnCl but irreversible for (DPPF$_8$)MnCl, (DPPCl$_{12}$)MnCl, (DPPF$_{20}$)MnCl, and (DPPF$_{28}$)MnCl. The current−voltage curves are better defined in CH_2Cl_2 (see Figure 5 for DPP and DPP(CF_3)$_4$ derivatives) than in PhCN, and a summary of the half-wave potentials in this later solvent is given in Table 5. As expected, the $E_{1/2}$ for the first oxidation of the compounds shifts positively with increase in the electron-withdrawing ability of the substituents so that (DPPF$_{28}$)MnCl is thus 540 mV more difficult to oxidize than (DPP)MnCl. This trend fits what would be predicted on the basis of simple substituent effects.

Electroreduction in PhCN. Each Mn(III) porphyrin undergoes a global three electron reduction, with the exact potentials and mechanism depending upon the degree of substitution of the macrocycle. Earlier studies on a variety of Mn(III) porphyrins have demonstrated that the electroreductions are reversible in strongly bonding solvents such as DMSO or pyridine but irreversible in a weakly bonding solvent such as PhCN or CH_2Cl_2.[39−42] This is also the case for the DPP derivatives which show a reversible to quasireversible Mn(III)/Mn(II) reaction in PhCN, followed by two sets of electrode reactions which lead to a Mn(II) π anion radical and then to a Mn(II) dianion. The first set of reactions involves the reduction of [(P)MnCl]$^-$ and (P)Mn, while the second involves the reduction of [(P)MnCl]$^{2-}$ and [(P)Mn]$^-$ as shown in Scheme 1 where the upper pathway is for porphyrins with a bound Cl$^-$ axial ligand and the lower for compounds without a bound Cl$^-$ axial ligand.

Table 5. Half-Wave Potentials (V vs SCE) for Oxidation of Manganese Porphyrins in CH_2Cl_2, 0.1 M TBAP

compd	1st oxdn	compd	1st oxdn
(DPP)MnCl	0.92	(DPPF$_8$)MnCl	1.14
(DPPF$_4$)MnCl	0.95	(DPPCl$_{12}$)MnCl	1.18
(DPPBr$_4$)MnCl	0.97	(DPPF$_{20}$)MnCl	1.11[a]−1.36[a]
(DPP(CF_3)$_4$)MnCl	1.03	(DPPF$_{28}$)MnCl	1.46[a]
(DPPCl$_8$)MnCl	1.10		

[a] E_{pa} at 0.1 V/s.

Scheme 1

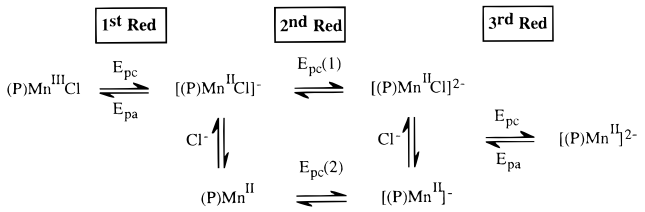

The ratio between the first two reduction products of (P)MnCl in solution, i.e., [(P)MnCl]$^-$ and (P)Mn, varies with the basicity of the macrocycle. (DPP(CF_3)$_4$)MnCl and (DPPCl$_8$)MnCl are reduced almost exclusively to (P)Mn (see Table 6) whereas (DPPF$_{20}$)MnCl and (DPPF$_{28}$)MnCl are reduced almost exclusively to [(P)MnCl]$^-$ after which Cl$^-$ may or may not dissociate from the Mn(II) derivative depending upon the specific compound, the time scale of the measurement (which depends upon the scan rate), and the presence or absence of (TBA)Cl added to solution. Because the equilibrium between the bound and the unbound forms of the Mn(II) porphyrin are quite sensitive to the experimental conditions, only the cathodic peak potentials, $E_{pc}(1)$ for [(P)MnCl]$^-$ and $E_{pc}(2)$ for (P)Mn, are listed in Table 6.

The difference between the two cathodic peak potentials for the second reduction, $E_{pc}(1)$ and $E_{pc}(2)$, ranges from 90 to 210 mV. A difference of 60 mV would be expected per each 10-fold increase in the (P)Mn^{II} binding constants with Cl$^-$ (see Scheme 2), and the absolute potential difference between $E_{pc}(2)$ and $E_{pc}(1)$ thus provides a qualitative indication of K for reaction 2 which ranges from about $10^{1.5}$ to $10^{3.5}$ depending upon the compound.

A shift of the equilibrium between four-coordinate (P)Mn and five-coordinate [(P)MnCl]$^-$ can easily be accomplished by addition of excess (TBA)Cl to the PhCN solution, and an example of the resulting current−voltage curve is shown in Figure 6

(40) Kadish, K. M.; Sweetland, M.; Cheng, J. S. *Inorg. Chem.* **1978**, *17*, 7, 2795−2797.
(41) Kadish, K. M.; Kelly, S. *Inorg. Chem.* **1979**, *18*, 2968−2971.
(42) Guilard, R.; Jagerovic, N.; Barbe, J. M.; Liu, Y. H.; Perrot, I.; Naillon, C.; Van Caemelbecke, E.; Kadish, K. M. *Polyhedron* **1995**, *14*, 3041−3050.

Table 6. Peak Potentials (V vs SCE) for Reduction (E_{pc}) and Reoxidation (E_{pa}) of Manganese Porphyrins in PhCN, 0.1 M TBAP (Scan Rate = 0.1 V/s)

	1st redn[a]				2nd redn[a,b]			3rd redn[a]	
compd	E_{pc}	E_{pa}	$E_{1/2}$	ΔE_p	$E_{pc}(1)$	$E_{pc}(2)$	ΔE_{pc}	E_{pc}	E_{pa}
(DPP)MnCl	−0.43	−0.30	−0.36	0.13	−1.55	−1.64	0.09	−1.89	−1.80
($DPPCl_8$)MnCl	−0.46	−0.20[c]	−0.33	0.26	−1.30	*d*		−1.72	−1.63
($DPPF_4$)MnCl	−0.42	−0.24	−0.33	0.18	−1.50	−1.60	0.10	∼−1.90	
($DPPBr_4$)MnCl	−0.42	−0.19	−0.25	0.13	−1.46	−1.54	0.09	−1.82	
($DPPF_8$)MnCl	−0.44	−0.10	−0.27	0.34	−1.30	−1.51	0.21	−1.67	−1.54
($DPP(CF_3)_4$)MnCl	−0.42	−0.07	−0.24	0.35	−1.46	*d*		∼−1.75	
($DPPCl_{12}$)MnCl	−0.28	−0.03	−0.15	0.25	−1.37	−1.52	0.15	−1.74	−1.62
($DPPF_{20}$)MnCl	−0.22	0.30	0.04	0.52	*e*	−1.19		−1.44	−1.31
($DPPF_{28}$)MnCl	−0.17	0.36	0.10	0.53	*e*	−1.08		−1.46	−1.23

[a] See Scheme 1 for location of E_{pc} and E_{pa}. [b] $E_{pc}(2)$ due to reduction of $[(P)MnCl]^-$ and $E_{pc}(1)$ due to reduction of (P)Mn. See text for additional details. [c] Additional electrode process seen at $E_{pc} = -0.32$ V. [d] $[(P)Mn^{II}Cl]^-$ not observed on the cyclic voltammetry time scale. [e] (P)Mn not observed on cyclic voltammetry time scale.

Scheme 2

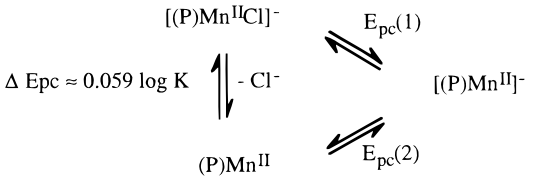

for the case of ($DPPF_{20}$)MnCl which, under these conditions, is reduced first to $[(DPPF_{20})MnCl]^-$ ($E_{pc} = -0.22$ V) and then to $[(DPPF_{20})MnCl]^{2-}$ ($E_{pc} = -1.19$ V) according to the upper pathway shown in Scheme 1. The changeover from a reaction involving reduction of $[(DPPF_{20})MnCl]^-$ at −1.19 V and reoxidation of $[(DPPF_{20})Mn]^-$ at −0.92 V in solutions of 0.1 M TBAP (Figure 6a) to one involving reduction of $[(DPPF_{20})MnCl]^-$ at −1.22 V and reoxidation of $[(DPPF_{20})MnCl]^{2-}$ at −1.10 V in solutions containing 0.1 M (TBA)Cl (Figure 6b) is consistent with strong chloride-binding to the manganese(II) π anion radical. The formation of a chloride bound Mn(II) follows what has been proposed for related $[(TPP)MnCl]^-$ derivatives in nonbonding or weakly bonding solvents,[43] but the binding of an anionic ligand to Mn(II) π anion radicals has not previously been shown to occur with compounds containing other porphyrin macrocycles.

The nature of the products formed after the second and third reduction of the manganese derivatives was not examined in detail, but on the basis of data published for other manganese porphyrins,[42−47] both reductions can be assigned as involving the conjugated porphyrin π ring system to give Mn(II) π anion radicals and dianions. The third reduction is quasireversible to reversible in PhCN, and the measured values of E_{pc} and E_{pa} are given in Table 6 without attempts to assign the nature of the axial ligand on either the reactant or the product of these reactions.

Electroreduction in Pyridine. Eight of the nine investigated (P)MnCl complexes undergo three well-defined reductions in pyridine (the $DPPCl_8$ compound undergoes two reductions), and an example of the resulting cyclic voltammogram is shown in Figure 7 for the case of (DPP)MnCl and ($DPPCl_{12}$)MnCl. The electrode reactions are all reversible to quasireversible, and no

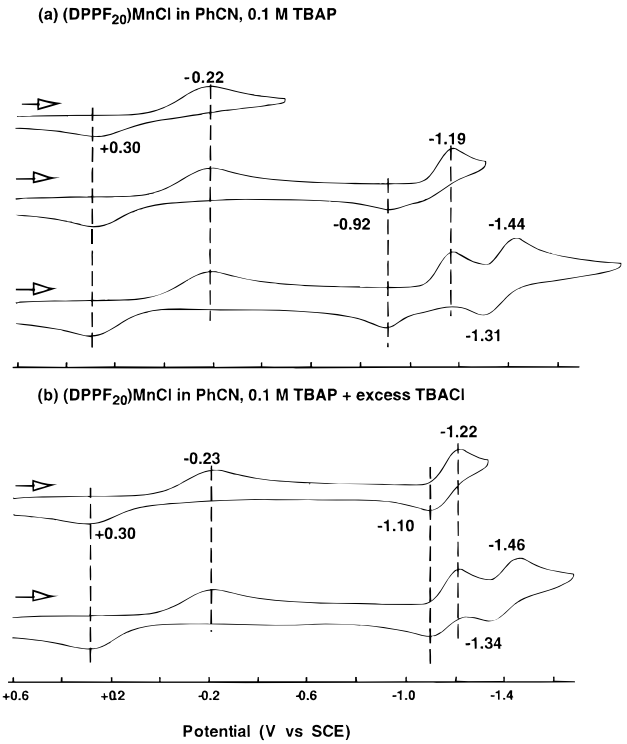

Figure 6. Cyclic voltammograms of ($DPPF_{20}$)MnCl in PhCN, 0.1 M TBAP (a) before and (b) after addition of (TBA)Cl. Scan rate = 0.1 V/s.

chemical reactions other than fast ligand exchange seem to be associated with any of the electrochemical processes.

The first reduction of (DPP)MnCl in pyridine occurs at $E_{1/2} = -0.41$ V, a value which is negatively shifted by 180 mV with respect to $E_{1/2}$ for the first reduction of (TPP)MnCl under the same solution conditions.[43] This result contrasts with the second and third reductions, where an opposite trend is observed between (DPP)MnCl and (TPP)MnCl; i.e., the second and third reductions of (DPP)MnCl are shifted positively (by 80 and 190 mV) with respect to the same electrode reactions of (TPP)MnCl. Consequently, the potential gap between the first two reductions of (DPP)MnCl in pyridine (0.83 V) is smaller than the potential gap between the first two reductions of (TPP)MnCl in pyridine (1.09 V). A smaller gap is also seen for the other eight DPP derivatives, where the $\Delta E_{1/2}$ between the first and second electron-transfer steps ranges from 0.77 to 0.93 V (see Table 7).

The electrochemistry of (TPP)MnCl in neat pyridine has been well-documented in the literature.[42,43,47] The compound, which exists[43] as the six-coordinate $[(TPP)Mn(py)_2]^+$, shows three

(43) Kelly, S. L.; Kadish, K. M. *Inorg. Chem.* **1982**, *21*, 3631−3639.
(44) Boucher, L. J. *Coord. Chem. Rev.* **1972**, *7*, 289−329.
(45) Felton, R. H.; Yu, N. T. In *The Porphyrins*; Dolphin, D., Ed.; Academic Press: New York, 1978; Vol. 3, pp 347−393.
(46) Fuhrhop, R. H. in *Porphyrins and Metalloporphyrins*; Smith, K. M., Ed.; Elsevier: New York, 1978; pp 593−623.
(47) Van Caemelbecke, E.; Kutner, W.; Kadish, K. M. *Inorg. Chem.* **1993**, *32*, 438−444.

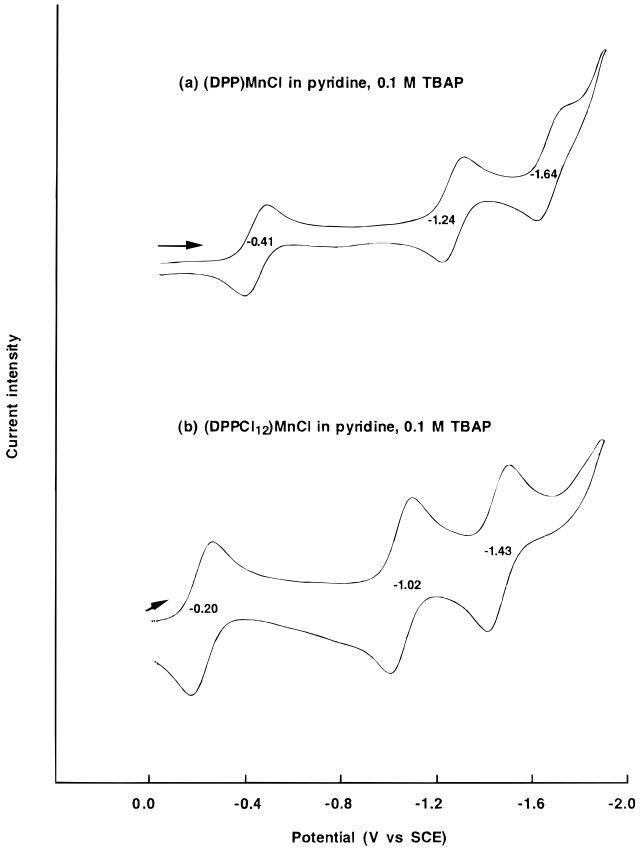

Figure 7. Cyclic voltammograms of (a) (DPP)MnCl and (b) ($DPPCl_{12}$)MnCl in pyridine, 0.1 M TBAP. Scan rate = 0.1 V/s.

Table 7. Half-Wave Potentials (V vs SCE) for Reduction of Manganese Porphyrins in Pyridine, 0.1 M TBAP

	redn				
compound	1st	2nd	3rd	Δ(2−1)	Δ(3−2)
(DPP)MnCl	−0.41	−1.24	−1.64	0.83	0.40
($DPPCl_8$)MnCl	−0.40	−1.22		0.82	
($DPPF_4$)MnCl	−0.37	−1.18	−1.66[a]	0.81	0.48
($DPPBr_4$)MnCl	−0.33	−1.12	−1.50	0.79	0.38
($DPPF_8$)MnCl	−0.28	−1.16	−1.58	0.88	0.42
($DPP(CF_3)_4$)MnCl	−0.28	−1.05	−1.52[a]	0.77	0.47
($DPPCl_{12}$)MnCl	−0.20	−1.02	−1.43	0.82	0.41
($DPPF_{20}$)MnCl	0.02	−0.88	−1.35	0.90	0.47
($DPPF_{28}$)MnCl	0.02[b]	−0.91[b]	−1.35[b]	0.93	0.44

[a] E_{pc} at 0.1 V/s. [b] Values obtained in CH_2Cl_2 containing 0.1 M TBAP and 160 equiv of pyridine.

well-defined, one-electron-transfer steps at $E_{1/2} = -0.23$, -1.32 and -1.83 V. The first reduction involves the Mn(III)/Mn(II) couple, while the following two involve the stepwise addition of electrons to the conjugated porphyrin macrocycle to generate a porphyrin π anion radical and dianion, respectively.[42,43,47] The electrochemistry of each DPP derivative in pyridine resembles

Scheme 3

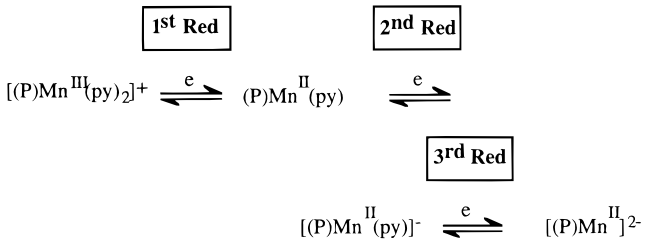

that of (TPP)MnCl and other chloromanganese(III) porphyrins[48] in that three reversible processes are observed (see $E_{1/2}$ values in Table 7). Spectroscopic data of the different DPP derivatives[49] suggest that all of the compounds exist as six-coordinate $[(P)Mn(py)_2]^+$ complexes in neat pyridine or in CH_2Cl_2/py mixtures this solvent and that they are reduced via the electron-transfer mechanism shown by Scheme 3.

Summary

Each (P)MnCl derivative can exist in five different oxidation states. All of the compounds are stable in their neutral form as well as after the addition of three electrons to generate a Mn(II) porphyrin dianion, but they show only transient stability in their singly oxidized form when dissolved in CH_2Cl_2 or PhCN containing 0.1 M TBAP. UV−visible and EPR spectroscopy of the complexes in CH_2Cl_2 under ozone suggests a Mn(IV) oxidation state in solution, and a Mn(IV) species may also be obtained by thin-layer spectoelectrochemistry.

A detailed characterization of the oxidation products under the electrochemical conditions was hampered by the occurrence of one or more coupled chemical reactions, and this contrasts with the results in CH_2Cl_2 solutions under ozone where the compounds are quite stable and can be isolated in the solid state. Attempts to crystallize the solid-state products obtained after ozonation of the manganese(III) dodecaphenylporphyrins have so far been unsuccessful, but EXAFS studies are currently underway to elucidate the structure of the isolated species in the solid state.

Acknowledgment. The support of the CNRS (R.G.), the Robert A. Welch Foundation (K.M.K.; Grant E-680), and the National Institute of Health (K.M.S.; Grant NIH HL-22252) is gratefully acknowledged.

Supporting Information Available: Tables of crystal data and structure refinement parameters, atomic coordinates and equivalent isotropic displacement parameters, bond lengths and angles, anisotropic displacement parameters, and coordinates and isotropic displacement parameters of hydrogen atoms for the ($DPPF_{20}$)MnCl complex (16 pages). Ordering information is given on any current masthead page.

IC970717W

(48) Autret, M.; Ou, Z. P.; Antonini, A.; Boschi, T.; Tagliatesta, P.; Kadish, K. M. *J. Chem. Soc., Dalton Trans.* **1996**, 2793−2797.
(49) Kadish, K. M., Unpublished results.